UNIVERSITY OF CALIFORNIA, SAN DIEGO

A Comprehensive Study of the Dzhanibekov and Tennis Racket Phenomena

A Thesis submitted in partial satisfaction of the requirements
for the degree Master of Science

in

Engineering Sciences (Mechanical Engineering)

by

Takeyuki Ono

Committee in charge:

Professor Hidenori Murakami, Chair
Professor Nathan Delson
Professor Michael Holst

2017

The Thesis of Takeyuki Ono is approved, and it is acceptable in quality and form for publication on microfilm and electronically:

Chair

University of California, San Diego

2017

TABLE OF CONTENTS

LIST OF FIGURES

ACKNOWLEDGEMENTS

I would first like to express my sincere gratitude to my advisor Professor Hidenori Murakami for the continuous support of my M.S. study and research, for his patience, motivation, enthusiasm, and immense knowledge. His guidance helped me throughout research and writing of this thesis.

I would like to thank Mr. Oscar Rios for all the support and encouragement he gave me. Without his precious guidance and feedback, it would not be possible to conduct this research.

I would also like to thank Professor Thomas J. Impelluso, Department of Mechanical and Marine Engineering, Western Norway University of Applied Science, Bergen, Norway, for generously sharing his time and knowledge in our cooperative work.

Chapter 2 and 3 in part, include the following published paper:

Rios, O., Ono, T., Murakami, H., and Impelluso, J. T., 2016, "An Analytical and Geometrical Study of the Dzhanibekov and Tennis Racket Phenomena," ASME Paper No. IMECE2016-65570. The thesis author was the principal researcher of this paper.

VITA

2017 Master of Science in Engineering Sciences (Mechanical Engineering)

University of California, San Diego, La Jolla, CA

2012-2017 Japan Ground Self-Defense Force

2012 Bachelor of Science in Mechanical Engineering

The National Defense Academy, Yokosuka, Japan

PUBLICATIONS

Rios, O., Ono, T., Murakami, H., and Impelluso, J. T., 2016, "An Analytical and Geometrical Study of the Dzhanibekov and Tennis Racket Phenomena," ASME Paper No. IMECE2016-65570.

Rios, O., Ono, T., Murakami, H., 2016, "Development of Active Mechanical Models for Flexible Robots to Duplicate the Motion of Inch Worms and Snakes," ASME Paper No. IMECE2016-65550.

ABSTRACT OF THE THESIS

A Comprehensive Study of the Dzhanibekov and Tennis Racket Phenomena

by

Takeyuki Ono

Master of Science in Engineering Sciences (Mechanical Engineering)

University of California, San Diego, 2017

Professor Hidenori Murakami, Chair

The Dzhanibekov and tennis racket phenomena are described by the torque-free rotation of a rigid body with three distinct principal moment of inertia values and angular velocity components. In these phenomena, rotations about the largest and smallest principal moments of inertia create stable rotations. However, when rotating about the intermediate principal moment of inertia, an unstable rotation is produced that leads to the basis of these

phenomena. In this thesis, the above phenomena are examined and explained analytically, geometrically, and numerically. In addition, the analysis is applied to a satellite system to observe the change in trajectory as the solar panels and reflectors are deployed. In the derivation, the Euler torque-free equations for a rotating rigid body are formulated using the moving frame method. The derived equations are then non-dimensionalized and a complete analytical solution, including an expression for the non-dimensional period, is presented. Furthermore, the axisymmetric cases and the effect of varying intermediate principal moment of inertia are examined. Lastly, the analytical expressions are compared with the numerical simulation to validate the results. The complete solution is then summarized and shown to clearly demonstrate that the conservation of angular momentum is indeed preserved in the phenomena.

CHAPTER 1: INTRODUCTION

In 1985, Vladimir Dzhanibekov, a Russian astronaut, conducted experiments in the space station concerning the rotation of a rigid body with three distinct principal moment of inertia values. As presented by Dzhanibekov, the rotation of a rigid body (dictionary, wing nut, box) about the intermediate moment of inertia causes the initial spin axis to rotate. Similar phenomenon has been observed on earth with a tennis racket and table tennis paddle, both of which produced similar results to Dzhanibekov's experiments [1, 2].

The equations governing rotational motion of a rigid body are referred to as Euler's equations, named after Leonhard Euler (1707-1783), who developed rigid body dynamics. As a special case, he investigated the torque-free rotation of a rigid body. Both the Dzhanibekov and the tennis racket phenomena can be governed by the torque-free Euler equations. The moving frame method will be used to show a clear derivation of the equations that govern this seemingly non-trivial behavior of the tennis racket and the Dzhanibekov experiments.

Analytical solutions of the torque-free Euler equations have been previously presented. Wittenburg demonstrated the analytical solution of Euler's equations using Jacobi elliptic functions, but with respect to the angular velocity components [3, 4]. Ashbaugh et al. also reported the analytical solution using Jacobi elliptic function for the tennis racket experiments by solving Euler's equations with respect to the momentum components, but no intermediate steps were shown in their derivation [5]. Previous work by Murakami et al. presented a numerical and geometrical explanation of the Dzhanibekov and tennis racket phenomena [6]. In this thesis, a complete non-dimensionalized analytical solution, including an expression for the non-dimensional period of the trajectory, is

presented by addressing analytical components. Furthermore, the transition is examined as the moment of inertia about the spin axis is varied when an initially spinning satellite deploys its solar panels.

CHAPTER 2: FORMULATION AND ANALYTICAL SOLUTION OF THE TORQUE-FREE RIGID BODY ROTATION

2.1 Formulation of Euler's Equation using the Moving Frame Method

The Euler torque-free equations for a rigid body are formulated by using the moving frame method. The moving frame method explicitly states the coordinate vector basis when expressing vectors to easily distinguish between an inertial and a moving frame observer. Firstly, a fixed inertial coordinate system $\{x_1 \;\; x_2 \;\; x_3\}$ and its corresponding orthonormal vector basis $\mathbf{e}^I \equiv (\mathbf{e}_1^I \;\; \mathbf{e}_2^I \;\; \mathbf{e}_3^I)$ are introduced with the origin at a specified point in Euclidean three-space, $\mathbb{R}^3$. Next, a body-attached principal coordinate system $\{s_1 \;\; s_2 \;\; s_3\}$ and its corresponding orthonormal vector basis $\mathbf{e}(t) \equiv (\mathbf{e}_1(t) \;\; \mathbf{e}_2(t) \;\; \mathbf{e}_3(t))$ are established in the directions of the body's principal axes. As shown in Figure 2.1, it is convenient to choose the inertial coordinate system to be the body-attached coordinate system at time $t = 0$, $\mathbf{e}^I = \mathbf{e}(0)$.

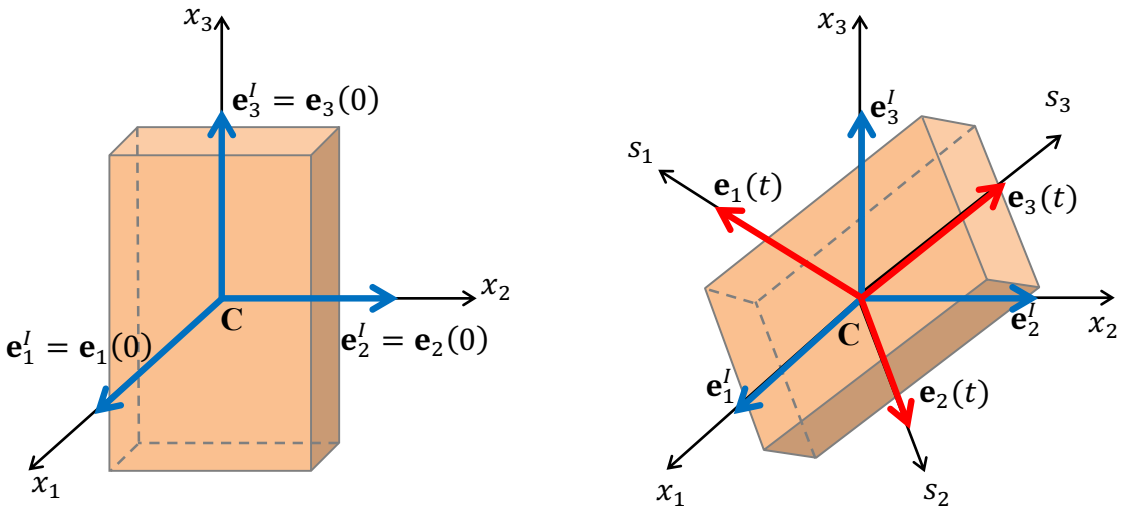

Figure 2.1: A fixed inertial coordinate system and a body-attached principal coordinate system

The vector basis is explicitly written in order to represent vectors and identify the coordinate system. In addition, the formulation is facilitated by adopting Frankel's compact notation [7], in which the vector basis $\mathbf{e}(t) \equiv (\mathbf{e}_1(t)\ \mathbf{e}_2(t)\ \mathbf{e}_3(t))$ is expressed by a 1×3 row matrix, and the components are expressed by a 3×1 column matrix [8].

To begin the derivation of Euler's equations, a relationship between the current body-attached frame and the inertial frame is established through a 3×3 rotation matrix $R(t)$.

$$\mathbf{e}(t) = \mathbf{e}^I R(t) \tag{1}$$

It should further be noted that rotation matrices, $R(t)$ belong to the special orthogonal group, SO (3), and thus $\big(R(t)\big)^T = \big(R(t)\big)^{-1}$.

$$\mathbf{e}^I = \mathbf{e}(t)\big(R(t)\big)^T \tag{2}$$

To obtain the angular velocity of the body, the time derivative of the body-attached frame is taken, and Eq. (2) is used to relate the expression back to its corresponding frame.

$$\dot{\mathbf{e}}(t) = \mathbf{e}^I \dot{R}(t) = \mathbf{e}(t)\big(R(t)\big)^T \dot{R}(t) = \mathbf{e}(t)\overleftrightarrow{\omega(t)} \tag{3}$$

The time rate of the body-attached frame produces a 3×3 skew-symmetric matrix known as the angular velocity matrix $\overleftrightarrow{\omega(t)}$

$$\overleftrightarrow{\omega(t)} \equiv \big(R(t)\big)^T \dot{R}(t) \equiv \begin{bmatrix} 0 & -\omega_3(t) & \omega_2(t) \\ \omega_3(t) & 0 & -\omega_1(t) \\ -\omega_2(t) & \omega_1(t) & 0 \end{bmatrix} \tag{4}$$

from which the angular velocity components with respect to the moving body can be obtained by observing a one-to-one relation between 3×3 skew-symmetric matrices in the Lie algebra of SO (3) and angular velocity vectors in $\mathbb{R}^3$.

$$\boldsymbol{\omega}(t) = \mathbf{e}(t)\omega(t) \equiv \begin{pmatrix}\mathbf{e}_1(t) & \mathbf{e}_2(t) & \mathbf{e}_3(t)\end{pmatrix}\begin{pmatrix}\omega_1(t)\\ \omega_2(t)\\ \omega_3(t)\end{pmatrix} \tag{5}$$

Since the moving frame coincides with body's principal axis, the mass moment of inertia matrix can be expressed as a diagonal 3×3 matrix as in Eq. (6) below. To be noted, the mass moment of inertia values will follow $J_{1C} > J_{2C} > J_{3C}$.

$$J_C = \begin{bmatrix}J_{1C} & 0 & 0\\ 0 & J_{2C} & 0\\ 0 & 0 & J_{3C}\end{bmatrix} \tag{6}$$

The angular momentum vector about the center of mass, $\boldsymbol{H}_C(t)$, can now be expressed with respect to the body attached or moving frame:

$$\begin{aligned}\boldsymbol{H}_C(t) &= \mathbf{e}(t)\, J_C\omega(t) = \mathbf{e}(t)H_C(t)\\ &\equiv \begin{pmatrix}\mathbf{e}_1(t) & \mathbf{e}_2(t) & \mathbf{e}_3(t)\end{pmatrix}\begin{pmatrix}H_{1c}(t)\\ H_{2c}(t)\\ H_{3c}(t)\end{pmatrix}\end{aligned} \tag{7}$$

where the components of the angular momentum are expressed with the product between the principal mass moment of inertia matrix and the angular velocity components as:

$$\begin{pmatrix}H_{1c}(t)\\ H_{2c}(t)\\ H_{3c}(t)\end{pmatrix} = \begin{bmatrix}J_{1C} & 0 & 0\\ 0 & J_{2C} & 0\\ 0 & 0 & J_{3C}\end{bmatrix}\begin{pmatrix}\omega_1(t)\\ \omega_2(t)\\ \omega_3(t)\end{pmatrix}. \tag{8}$$

The frame of reference can easily be changed to that of an inertial frame since the vector basis is explicitly stated. Expressing the angular momentum vector with respect to the inertial frame observer is done by a simple substitution using Eq. (1) above:

$$\boldsymbol{H}_C(t) = \mathbf{e}^I R(t)\, J_C\omega(t) = \mathbf{e}^I H_C^I(t). \tag{9}$$

To obtain Euler's torque-free equations, the time derivative of the angular momentum is taken and equated to zero. Note, without explicitly stating the vector basis when expressing

the angular momentum, confusion can arise when obtaining the time rate. Taking the time derivative of Eq. (7) results in the following expression for the angular momentum with respect to the moving frame:

$$\dot{\boldsymbol{H}}_c(t) = \mathbf{e}(t)\dot{H}_c(t) + \dot{\mathbf{e}}(t)H_c(t) = 0. \tag{10}$$

The substitution of Eq. (3) into Eq. (10) above for $\dot{\mathbf{e}}(t)$ results in the governing equations for a torque free rotation of a rigid body:

$$\dot{\boldsymbol{H}}(t) = \mathbf{e}(t)\left\{\dot{H}_c(t) + \overleftrightarrow{\omega(t)}H_c(t)\right\} = 0. \tag{11}$$

Equation (11) above, expressed in component form, results in three first order differential equations that govern the torque-free rotation of a rigid body

$$\dot{H}_{1C}(t) - \omega_3(t)H_{2C}(t) + \omega_2(t)H_{3C}(t) = 0, \tag{12a}$$

$$\dot{H}_{2C}(t) + \omega_3(t)H_{1C}(t) - \omega_1(t)H_{3C}(t) = 0, \tag{12b}$$

$$\dot{H}_{3C}(t) - \omega_2(t)H_{1C}(t) + \omega_1(t)H_{2C}(t) = 0. \tag{12c}$$

By substituting for the angular velocity components in the above three differential equations using Eq. (8), the equations can be expressed by using only the mass moments of inertia and the angular momenta

$$\dot{H}_{1C}(t) + \left(\frac{1}{J_{2C}} - \frac{1}{J_{3C}}\right)H_{2C}(t)H_{3C}(t) = 0, \tag{13a}$$

$$\dot{H}_{2C}(t) + \left(\frac{1}{J_{3C}} - \frac{1}{J_{1C}}\right)H_{1C}(t)H_{3C}(t) = 0, \tag{13b}$$

$$\dot{H}_{3C}(t) + \left(\frac{1}{J_{1C}} - \frac{1}{J_{2C}}\right)H_{1C}(t)H_{2C}(t) = 0. \tag{13c}$$

As can be seen, the moving frame method provides a clear derivation and avoids any user confusion by explicitly stating the vector basis. It also provides a succinct and easy way of changing the frame of reference through the use of rotation matrices.

2.2 Analytical Solution of Euler's Equation

Euler confirmed that four quantities were conserved: the kinetic energy and the three angular momentum components. He also noted that the length of the angular momentum vector remained constant. From these observations, the conservation of rotational kinetic energy:

$$\frac{\left(H_{1C}(t)\right)^2}{J_{1C}} + \frac{\left(H_{2C}(t)\right)^2}{J_{2C}} + \frac{\left(H_{3C}(t)\right)^2}{J_{3C}} = 2K_0, \tag{14}$$

and the conservation of the magnitude of the angular momentum vector is expressed as:

$$\left(H_{1C}(t)\right)^2 + \left(H_{2C}(t)\right)^2 + \left(H_{3C}(t)\right)^2 = \|\boldsymbol{H}_C(0)\|^2. \tag{15}$$

In the above, K_0 represents the initial rotational kinetic energy, calculated from the initial conditions and body parameters as follows:

$$K_0 = \frac{1}{2}\left\{J_{1C}\left(\omega_1(0)\right)^2 + J_{2C}\left(\omega_2(0)\right)^2 + J_{3C}\left(\omega_3(0)\right)^2\right\}, \tag{16}$$

and the norm $\|\boldsymbol{H}_C(t)\|$ of the angular momentum vector remains the magnitude at $t = 0$.

Euler observed from his equations that three steady-state solutions referred to as permanent rotation states exist

$$\omega_1(t) = \omega_0,\ \omega_2(t) = \omega_3(t) = 0 \tag{17a}$$

$$\omega_1(t) = 0,\ \omega_2(t) = \omega_0,\ \omega_3(t) = 0 \tag{17b}$$

$$\omega_1(t) = \omega_2(t) = 0,\ \omega_3(t) = \omega_0, \tag{17c}$$

where $\omega_0$is a constant.

In certain cases, when a dominant angular velocity is applied about one principal axis to induce a state of permanent rotation, the initial angular velocity deviates slightly from the state of permanent rotation. In other words, in addition to the dominant component about

the principal axis, the initial angular velocity includes small angular-velocity components about other axes. To account for the slight perturbation of initial conditions, the stability of the angular velocity components near the permanent rotation states must be examined.

Geometrically, the energy ellipsoid expressed with respect to the H_{1C}, H_{2C}, and H_{3C}-axis can be constructed using Eq. (14):

$$\left(\frac{H_{1C}(t)}{\sqrt{2K_0J_{1C}}}\right)^2+\left(\frac{H_{2C}(t)}{\sqrt{2K_0J_{2C}}}\right)^2+\left(\frac{H_{3C}(t)}{\sqrt{2K_0J_{3C}}}\right)^2=1, \tag{18}$$

and the angular momentum sphere can be defined as:

$$\left(H_{1C}(t)\right)^2+\left(H_{2C}(t)\right)^2+\left(H_{3C}(t)\right)^2=2K_0D. \tag{19}$$

where *D* is a parameter, which changes the radius of the angular momentum sphere

$$D=\frac{\|\boldsymbol{H}_c(0)\|^2}{2K_0}. \tag{20}$$

Since the body-attached coordinate axes are defined so that the inequality of the mass moment of inertia $J_{1C}>J_{2C}>J_{3C}$ is satisfied, the following inequality for the parameter *D* is required:

$$J_{1C}\geq D\geq J_{3C}. \tag{21}$$

The intersection of the energy ellipsoid and the angular momentum sphere is the trajectory of the angular momentum vector with respect to the body attached coordinate frame. Louis Poinsot (1777-1859) in the 19th century, added a geometrical interpretation to Euler's analytical solution. He stated that the intersecting path of Eqs. (14) and (15) is the trajectory of the angular velocity vector with respect to the body attached coordinate frame. The collective curves of intersection, as the angular momentum ellipsoid is varied, are referred to as polhodes by Poinsot [9].

2.3 Non-dimensional Analytical Solution

The analytical solution to the non-dimensional Euler's equations with respect to the moving frame will be derived. Before doing so, the Euler's equations, the angular momentum sphere, and the energy ellipsoid will be non-dimensionalized. Non-dimensionalization will allow for an easier interpretation and visualization of the polhodes, producing a constant energy ellipsoid and an angular momentum sphere with a single parameter, which controls the radii of the sphere. The analytical solution of the non-dimensionalized Euler's equations will then be obtained through the use of elliptic functions for varying moment of inertia values and expression for the non-dimensional period of the trajectory will be obtained in the next section.

2.3.1 Non-dimensionalization of Euler's Equations

The non-dimensionalization process is presented for the angular momentum sphere and energy ellipsoid, defined in Eqs. (18) and (19). The non-dimensional angular momentum components, represented by over-bars, are obtained from the energy ellipsoid and angular momentum sphere by using the terms associated with the $H_{2C}(\mathrm{t})$ component

$$\overline{H}_{iC} = \frac{H_{iC}}{\sqrt{2K_0 J_{2c}}}, \qquad i = 1,2,3. \tag{22}$$

To obtain an expression for the non-dimensionalized time, a reference time t_r is established

$$t = t_r \bar{t}. \tag{23}$$

Substituting Eqs. (22) and (23) back into one of Euler's equations (Eq. (13a) was chosen):

$$\frac{1}{t_r}\sqrt{\frac{J_{2c}}{2K_0}}\,\frac{d}{d\bar{t}}\,\overline{H}_{1C}+\left(1-\frac{J_{2c}}{J_{3c}}\right)\overline{H}_{2C}\,\overline{H}_{3C}=0. \tag{24}$$

The expression for the reference time can thus be obtained from the first term above

$$\sqrt{\frac{J_{2c}}{2K_0}}=t_r. \tag{25}$$

Substituting Eq. (25) into Eq. (23), the non-dimensional expression for time is obtained:

$$\bar{t}=\sqrt{\frac{2K_0}{J_{2c}}}\;t. \tag{26}$$

The non-dimensional Euler's equations can now be expressed:

$$\frac{d}{d\bar{t}}\overline{H}_{1C}+\left(1-\frac{J_{2C}}{J_{3C}}\right)\overline{H}_{2C}\overline{H}_{3C}=0, \tag{27a}$$

$$\frac{d}{d\bar{t}}\overline{H}_{2C}+\left(\frac{J_{2C}}{J_{3C}}-\frac{J_{2C}}{J_{1C}}\right)\overline{H}_{3C}\,\overline{H}_{1C}=0, \tag{27b}$$

$$\frac{d}{d\bar{t}}\overline{H}_{3c}+\left(\frac{J_{2c}}{J_{1c}}-1\right)\overline{H}_{1c}\,\overline{H}_{2c}=0. \tag{27c}$$

Lastly, using Eqs. (18), (19), and (22), the non-dimensional constant energy ellipsoid and the non-dimensional angular momentum sphere result in Eqs. (28) and (29) respectively

$$\left(\frac{J_{2c}}{J_{1c}}\right)\left(\overline{H}_{1c}\right)^2+\left(\overline{H}_{2c}\right)^2+\left(\frac{J_{2c}}{J_{3c}}\right)\left(\overline{H}_{3c}\right)^2=1, \tag{28}$$

$$\left(\overline{H}_{1c}\right)^2+\left(\overline{H}_{2c}\right)^2+\left(\overline{H}_{3c}\right)^2=\overline{d}. \tag{29}$$

The variable $\overline{d}$, defined below, is the single parameter that is varied to control the radius of the angular momentum sphere

$$\overline{d}=D/J_{2c}\,. \tag{30}$$

From Eq. (21), the radius $\sqrt{\overline{d}}$ of the non-dimensional angular momentum sphere satisfies

the following inequality:

$$\frac{J_{3c}}{J_{2c}} \leq \overline{d} \leq \frac{J_{1c}}{J_{2c}}. \tag{31}$$

The above equations conclude the non-dimensionalization of relevant quantities.

2.3.2 Geometrical Solution

The intersections between the energy ellipsoid and the angular momentum sphere present the geometrical solutions for a body under torque-free motion.

Firstly, the projection of the intersections on to the $\overline{H}_{2c}$, $\overline{H}_{3c}$-plane is considered. The equation for the trajectory is obtained by eliminating $\overline{H}_{1c}$ from Eqs. (28) and (29)

$$\left(1-\frac{J_{2c}}{J_{1c}}\right)\left(\overline{H}_{2c}\right)^2+\left(\frac{J_{2c}}{J_{3c}}-\frac{J_{2c}}{J_{1c}}\right)\left(\overline{H}_{3c}\right)^2=\left(1-\frac{J_{2c}}{J_{1c}}\overline{d}\right)\geq 0. \tag{32}$$

From Eq. (31), the inequality of the right-hand side is obtained and the coefficients on the left-hand side are both positive. Hence, the above equation describes an ellipse if the right-hand side does not vanish, $\overline{d} < J_{1c}/J_{2c}$. If the right-hand side of Eq. (32) vanishes, $\overline{d} = J_{1c}/J_{2c}$, it shows the state of permanent rotation: $\overline{H}_{1c} = \sqrt{\overline{d}}$, $\overline{H}_{2c} = \overline{H}_{3c} = 0$.

Second, the projection on to the $\overline{H}_{1c}$, $\overline{H}_{2c}$-plane is considered. The equation for the trajectory is obtained by eliminating $\overline{H}_{3c}$ from Eqs. (28) and (29)

$$\left(\frac{J_{2c}}{J_{3c}}-\frac{J_{2c}}{J_{1c}}\right)\left(\overline{H}_{1c}\right)^2+\left(\frac{J_{2c}}{J_{3c}}-1\right)\left(\overline{H}_{2c}\right)^2=\left(\frac{J_{2c}}{J_{3c}}\overline{d}-1\right)\geq 0. \tag{33}$$

Here, the inequality on the right–hand side is obtained by using the inequality (31). Since the coefficients on the left-hand side are both positive, Eq. (33) represents an ellipse if the right-hand side does not vanish, $\overline{d} > J_{3c}/J_{2c}$. If the right-hand side of Eq. (33) vanishes, $\overline{d} = J_{3c}/J_{2c}$, it becomes a point showing the state of permanent rotation: $\overline{H}_{1c} = \overline{H}_{2c} = 0$,

$\overline{H}_{3c} = \sqrt{\overline{d}}$.

Finally, the projection on to the $\overline{H}_{1c}$, $\overline{H}_{3c}$-plane is considered. The equation for the trajectory is obtained by eliminating $\overline{H}_{2c}$ from Eqs. (28) and (29)

$$-\left(1-\frac{J_{2c}}{J_{1c}}\right)\left(\overline{H}_{1c}\right)^2+\left(\frac{J_{2c}}{J_{3c}}-1\right)\left(\overline{H}_{3c}\right)^2=1-\overline{d}. \tag{34}$$

Here, the coefficients in pairs of parentheses on the left-hand side are both positive. Then, Eq. (34) shows a hyperbola. The equations of its asymptotes are

$$\overline{H}_{3c}=\pm\sqrt{\frac{J_{3c}(J_{1c}-J_{2c})}{J_{1c}(J_{2c}-J_{3c})}}\overline{H}_{1c}. \tag{35}$$

If $\overline{d}<1$, the vertices and focal points of the hyperbola are on the $\overline{H}_{3c}$-axis in the projected plane. Therefore, on the energy ellipsoid, the trajectory is closed and circulates about the $\overline{H}_{3c}$-axis. On the contrary, if $\overline{d}>1$, the vertices and focal points of the hyperbola are on the $\overline{H}_{1c}$-axis in the projected plane. Therefore, on the energy ellipsoid, the trajectory is closed and circulates about the $\overline{H}_{1c}$-axis. If $\overline{d}=1$, the trajectory of Eq. (34) becomes Eq. (35). Then, Eq. (35) becomes separatrices. Furthermore, $\overline{H}_{1c}=\overline{H}_{3c}=0$ represents the state of permanent rotation, $\overline{H}_{2c}=1$. Figure 2.2 shows that angular momentum trajectories which are intersections between the non-dimensional energy ellipsoid and the non-dimensional angular momentum sphere.

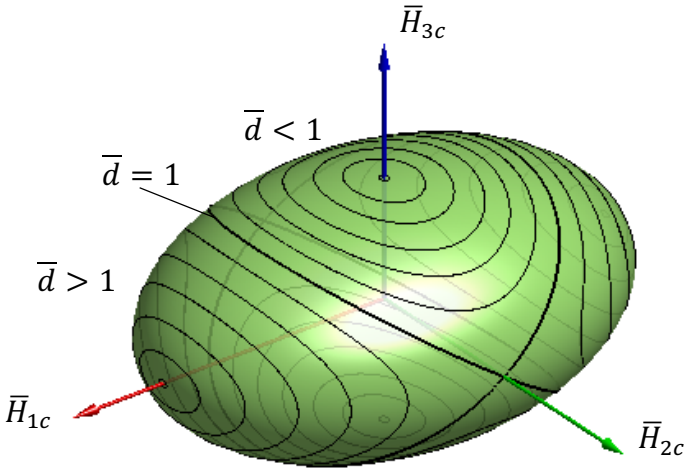

Figure 2.2: Polhodes on a non-dimensional energy ellipsoid

2.3.3 Solution of the non-dimensional Euler's Equation

First, from Eqs. (32) and (33), $\overline{H}_{1c}$ and $\overline{H}_{3c}$ can be solved as functions of $\overline{H}_{2c}$

$$\left(\overline{H}_{1c}\right)^2 = \frac{J_{1c}(J_{2c} - J_{3c})}{J_{2c}(J_{1c} - J_{3c})}\left(\overline{a}^2 - \left(\overline{H}_{2c}\right)^2\right), \tag{36}$$

$$\left(\overline{H}_{3c}\right)^2 = \frac{J_{3c}(J_{1c} - J_{2c})}{J_{2c}(J_{1c} - J_{3c})}\left(\overline{b}^2 - \left(\overline{H}_{2c}\right)^2\right), \tag{37}$$

where $\overline{a}^2$ and $\overline{b}^2$ are positive constants defined as follows:

$$\overline{a}^2 \equiv \frac{J_{2c}\overline{d} - J_{3c}}{J_{2c} - J_{3c}} = \frac{D - J_{3c}}{J_{2c} - J_{3c}}, \tag{38a}$$

$$\overline{b}^2 \equiv \frac{J_{1c} - J_{2c}\overline{d}}{J_{1c} - J_{2c}} = \frac{J_{1c} - D}{J_{1c} - J_{2c}}. \tag{38b}$$

From the above expressions, $\overline{a}^2$ and $\overline{b}^2$ can be said to satisfy the following relationship:

$$\overline{a}^2 - \overline{b}^2 = \frac{\left(\overline{d} - 1\right)\left(\frac{J_{1c}}{J_{2c}} - \frac{J_{3c}}{J_{2c}}\right)}{\left(1 - \frac{J_{3c}}{J_{2c}}\right)\left(\frac{J_{1c}}{J_{2c}} - 1\right)} = \frac{(D - J_{2c})(J_{1c} - J_{3c})}{(J_{2c} - J_{3c})(J_{1c} - J_{2c})}. \tag{39}$$

Next, the substitution of $\overline{H}_{1c}$ and $\overline{H}_{3c}$ from Eqs. (36) and (37) into the second non-

dimensional Euler equation and the use of the separation of variables method result in the following equation:

$$\frac{d\overline{H}_{2c}}{\sqrt{\left(\overline{a}^2-\left(\overline{H}_{2c}\right)^2\right)\left(\overline{b}^2-\left(\overline{H}_{2c}\right)^2\right)}}=-\sqrt{\frac{(J_{1c}-J_{2c})(J_{2c}-J_{3c})}{J_{1c}J_{3c}}}\,d\overline{t}. \tag{40}$$

To solve above equation, three cases need to be considered with regards to $\overline{a}$ and $\overline{b}$. Firstly, *Case 1*: $\overline{a}^2<\overline{b}^2$ which leads to $\overline{a}<\overline{b}$, $\overline{d}<1$, and $D<J_{2c}$ is considered. Altering Eq. (40) for the case at hand leads to the following equation:

$$\int\frac{d\left(\frac{\overline{H}_{2c}}{\overline{a}}\right)}{\sqrt{\left(1-\left(\frac{\overline{H}_{2c}}{\overline{a}}\right)^2\right)\left(1-\left(\frac{\overline{a}}{\overline{b}}\right)^2\left(\frac{\overline{H}_{2c}}{\overline{a}}\right)^2\right)}}=-\int\overline{b}\sqrt{\frac{(J_{1c}-J_{2c})(J_{2c}-J_{3c})}{J_{1c}J_{3c}}}\,d\overline{t}. \tag{41}$$

On the left-hand side, the integral is recognized to be an elliptic integral of the first kind. Therefore, by using Jacobi elliptic functions, an expression for $\overline{H}_{2c}$ can be obtained:

$$\overline{H}_{2c}=-\overline{a}\,\mathrm{sn}\left(\overline{\xi}\left(\overline{t}\right)\right), \tag{42}$$

where $\overline{\xi}\left(\overline{t}\right)$ is expressed below

$$\overline{\xi}\left(\overline{t}\right)=\overline{b}\sqrt{\frac{(J_{1c}-J_{2c})(J_{2c}-J_{3c})}{J_{1c}J_{3c}}}\left(\overline{t}-\overline{t}_0\right), \tag{43}$$

The solutions for $\overline{H}_{1c}$and $\overline{H}_{3c}$ are obtained by substituting Eq. (42) into Eqs. (36) and (37), and by using the addition theorems for the elliptic functions: $\mathrm{sn}^2\tau+\mathrm{cn}^2\tau=1$ and $\mathrm{dn}^2\tau+k^2\mathrm{sn}^2\tau=1$ where $k^2=\overline{a}^2/\overline{b}^2$ [10]

$$\overline{H}_{1c}=\pm\overline{a}\sqrt{\frac{J_{1c}(J_{2c}-J_{3c})}{J_{2c}(J_{1c}-J_{3c})}}\,\mathrm{cn}\left(\overline{\xi}\left(\overline{t}\right)\right), \tag{44}$$

$$\overline{H}_{3c} = \pm\overline{b}\sqrt{\frac{J_{3c}(J_{1c}-J_{2c})}{J_{2c}(J_{1c}-J_{3c})}}\,\mathrm{dn}\left(\overline{\xi}(\overline{t})\right). \tag{45}$$

The sign of each non-dimensional angular momentum component is determined from the signs of the initial conditions and by checking Euler's equation of motion. Therefore, if $\overline{H}_{3c} > 0$,

$$\overline{H}_{1c} = +\overline{a}\sqrt{\frac{J_{1c}(J_{2c}-J_{3c})}{J_{2c}(J_{1c}-J_{3c})}}\,\mathrm{cn}\left(\overline{\xi}(\overline{t})\right), \tag{46a}$$

$$\overline{H}_{2c} = -\overline{a}\,\mathrm{sn}\left(\overline{\xi}(\overline{t})\right), \tag{46b}$$

$$\overline{H}_{3c} = +\overline{b}\sqrt{\frac{J_{3c}(J_{1c}-J_{2c})}{J_{2c}(J_{1c}-J_{3c})}}\,\mathrm{dn}\left(\overline{\xi}(\overline{t})\right), \tag{46c}$$

and if $\overline{H}_{3c} < 0$,

$$\overline{H}_{1c} = -\overline{a}\sqrt{\frac{J_{1c}(J_{2c}-J_{3c})}{J_{2c}(J_{1c}-J_{3c})}}\,\mathrm{cn}\left(\overline{\xi}(\overline{t})\right), \tag{46d}$$

$$\overline{H}_{2c} = -\overline{a}\,\mathrm{sn}\left(\overline{\xi}(\overline{t})\right), \tag{46e}$$

$$\overline{H}_{3c} = -\overline{b}\sqrt{\frac{J_{3c}(J_{1c}-J_{2c})}{J_{2c}(J_{1c}-J_{3c})}}\,\mathrm{dn}\left(\overline{\xi}(\overline{t})\right), \tag{46f}$$

where $\overline{a}$ and $\overline{b}$ are expressed as

$$\overline{a} = \pm\sqrt{\frac{J_{2c}\overline{d}-J_{3c}}{J_{2c}-J_{3c}}} = \pm\sqrt{\frac{D-J_{3c}}{J_{2c}-J_{3c}}}, \tag{47a}$$

$$\overline{b} = \sqrt{\frac{J_{1c}-J_{2c}\overline{d}}{J_{1c}-J_{2c}}} = \sqrt{\frac{J_{1c}-D}{J_{1c}-J_{2c}}}. \tag{47b}$$

The non-dimensional period of the Jacobi elliptic functions is obtained from the complete elliptic integral of the first kind where sn and cn are *4K* periodic and dn is *2K* periodic. Using Eq. (43), the following equations can be written

$$4K\left(\frac{\overline{a}}{\overline{b}}\right) = \overline{b}\sqrt{\frac{(J_{1c}-J_{2c})(J_{2c}-J_{3c})}{J_{1c}J_{3c}}}\left(\overline{t}-\overline{t}_0\right), \tag{48a}$$

$$2K\left(\frac{\overline{a}}{\overline{b}}\right) = \overline{b}\sqrt{\frac{(J_{1c}-J_{2c})(J_{2c}-J_{3c})}{J_{1c}J_{3c}}}\left(\overline{t}-\overline{t}_0\right). \tag{48b}$$

The non-dimensional period can then be found by stating that the time shift corresponds to a period. The non-dimensional period for $\overline{H}_{1c}$ and $\overline{H}_{2c}$ becomes:

$$\overline{T} = \frac{4K\left(\frac{\overline{a}}{\overline{b}}\right)}{\overline{b}\sqrt{\frac{(J_{1c}-J_{2c})(J_{2c}-J_{3c})}{J_{1c}J_{3c}}}}, \tag{49a}$$

and the non-dimensional period for $\overline{H}_{3c}$ becomes:

$$\overline{T} = \frac{2K\left(\frac{\overline{a}}{\overline{b}}\right)}{\overline{b}\sqrt{\frac{(J_{1c}-J_{2c})(J_{2c}-J_{3c})}{J_{1c}J_{3c}}}}. \tag{49b}$$

Second, *Case 2*: $\overline{a}^2 > \overline{b}^2$ which leads to $\overline{a} > \overline{b}$, $\overline{d} > 1$, and $D > J_{2c}$ is considered. Equation (40) can thus be rewritten as:

$$\int \frac{d\left(\frac{\overline{H}_{2c}}{\overline{b}}\right)}{\sqrt{\left(1-\left(\frac{\overline{b}}{\overline{a}}\right)^2\left(\frac{\overline{H}_{2c}}{\overline{b}}\right)^2\right)\left(1-\left(\frac{\overline{H}_{2c}}{\overline{b}}\right)^2\right)}} = -\int \overline{a}\sqrt{\frac{(J_{1c}-J_{2c})(J_{2c}-J_{3c})}{J_{1c}J_{3c}}}\,d\overline{t}, \tag{50}$$

The solutions for the non-dimensional angular momentum and period are derived in the same manner as shown in *Case 1*. If $\overline{H}_{1c} > 0$,

$$\overline{H}_{1c} = +\overline{a}\sqrt{\frac{J_{1c}(J_{2c}-J_{3c})}{J_{2c}(J_{1c}-J_{3c})}}\,\mathrm{dn}\left(\overline{\eta}(\overline{t})\right), \tag{51a}$$

$$\overline{H}_{2c} = -\overline{b}\,\mathrm{sn}\left(\overline{\eta}(\overline{t})\right), \tag{51b}$$

$$\overline{H}_{3c} = +\overline{b}\sqrt{\frac{J_{3c}(J_{1c}-J_{2c})}{J_{2c}(J_{1c}-J_{3c})}}\,\mathrm{cn}\left(\overline{\eta}(\overline{t})\right), \tag{51c}$$

and if $\overline{H}_{1c} < 0$,

$$\overline{H}_{1c} = -\overline{a}\sqrt{\frac{J_{1c}(J_{2c}-J_{3c})}{J_{2c}(J_{1c}-J_{3c})}}\,\mathrm{dn}\left(\overline{\eta}(\overline{t})\right), \tag{51d}$$

$$\overline{H}_{2c} = -\overline{b}\,\mathrm{sn}\left(\overline{\eta}(\overline{t})\right), \tag{51e}$$

$$\overline{H}_{3c} = -\overline{b}\sqrt{\frac{J_{3c}(J_{1c}-J_{2c})}{J_{2c}(J_{1c}-J_{3c})}}\,\mathrm{cn}\left(\overline{\eta}(\overline{t})\right), \tag{51f}$$

where $\overline{\eta}(\overline{t})$, $\overline{a}$, and $\overline{b}$ are expressed below

$$\overline{\eta}(\overline{t}) = \overline{a}\sqrt{\frac{(J_{1c}-J_{2c})(J_{2c}-J_{3c})}{J_{1c}J_{3c}}}\,(\overline{t}-\overline{t}_0), \tag{52}$$

$$\overline{a} = \sqrt{\frac{J_{2c}\overline{d}-J_{3c}}{J_{2c}-J_{3c}}} = \sqrt{\frac{D-J_{3c}}{J_{2c}-J_{3c}}}, \tag{53a}$$

$$\overline{b} = \pm\sqrt{\frac{J_{1c}-J_{2c}\overline{d}}{J_{1c}-J_{2c}}} = \pm\sqrt{\frac{J_{1c}-D}{J_{1c}-J_{2c}}}. \tag{53b}$$

The non-dimensional period for $\overline{H}_{2c}$ and $\overline{H}_{3c}$ is written as:

$$\overline{T} = \frac{4K\left(\frac{\overline{b}}{\overline{a}}\right)}{\overline{a}\sqrt{\frac{(J_{1c}-J_{2c})(J_{2c}-J_{3c})}{J_{1c}J_{3c}}}}, \tag{54a}$$

and the non-dimensional period for $\overline{H}_{1c}$ is expressed as:

$$\overline{T} = \frac{2K\left(\frac{\overline{b}}{\overline{a}}\right)}{\overline{a}\sqrt{\frac{(J_{1c}-J_{2c})(J_{2c}-J_{3c})}{J_{1c}J_{3c}}}}, \tag{54b}$$

The complete elliptic integral can be evaluated using a polynomial approximation as presented by Abramowitz and Stegun [10].

Finally, *Case 3*: $\overline{a}^2 = \overline{b}^2$ which leads to $\overline{a} = \overline{b}$, $\overline{d} = 1$, and $D = J_{2C}$ is considered. In this case, Eq. (40) becomes

$$\frac{d\overline{H}_{2c}}{\overline{a}^2 - \left(\overline{H}_{2c}\right)^2} = -\sqrt{\frac{(J_{1c}-J_{2c})(J_{2c}-J_{3c})}{J_{1c}J_{3c}}}\, d\overline{t}. \tag{55}$$

Integrating the above expression results in Eq. (56) below

$$\tanh^{-1}\left(\overline{H}_{2c}/\overline{a}\right) = -\overline{a}\sqrt{\frac{(J_{1c}-J_{2c})(J_{2c}-J_{3c})}{J_{1c}J_{3c}}}\left(\overline{t}-\overline{t}_0\right). \tag{56}$$

To simplify the final expression for $\overline{H}_{2c}$, a time variable $\overline{\eta}(\overline{t})$ is introduced

$$\overline{\eta}(\overline{t}) = \overline{a}\sqrt{\frac{(J_{1c}-J_{2c})(J_{2c}-J_{3c})}{J_{1c}J_{3c}}}\left(\overline{t}-\overline{t}_0\right). \tag{57}$$

The final expression for $\overline{H}_{2c}$ for *Case 3* can thus be stated as below:

$$\overline{H}_{2c} = -\overline{a}\tanh\left(\overline{\eta}(\overline{t})\right). \tag{58}$$

The solutions for $\overline{H}_{1c}$and $\overline{H}_{3c}$ are obtained by substituting Eq. (58) into Eqs. (36) and

(37):

$$\overline{H}_{1c} = \pm\overline{a}\sqrt{\frac{J_{1c}(J_{2c}-J_{3c})}{J_{2c}(J_{1c}-J_{3c})}}\frac{1}{\cosh\left(\overline{\eta}(\overline{t})\right)}, \tag{59}$$

$$\overline{H}_{3c} = \pm\overline{a}\sqrt{\frac{J_{3c}(J_{1c}-J_{2c})}{J_{2c}(J_{1c}-J_{3c})}}\frac{1}{\cosh\left(\overline{\eta}(\overline{t})\right)}. \tag{60}$$

In this case, the solutions are not periodic whereas the solutions of *case 1* and *case 2* are periodic. Therefore, as $\overline{\eta}(\overline{t}) \to \infty$, $\overline{H}_{1c}$ and $\overline{H}_{3c}$ go to zero and $\overline{H}_{2c}$ approaches $-\overline{a}$. Also, as $\overline{d} \to 1$, the solutions of *case1* and *case2* converge on the solutions of *case3*.

2.3.4 Axisymmetric Cases

The analytical solutions for the axisymmetric cases are presented by taking the limit of the equations derived above. In these cases, a rigid body has two equal principal moments of inertia and the solutions are expressed with simpler form. Firstly, the case where the intermediate mass moment of inertia approaches the largest moment of inertia is considered. The intermediate mass moment of inertia J_2 near the largest moment of inertia J_1 can be expressed as follows using a small parameter ε, $|\varepsilon| \ll 1$:

$$J_2 = J_1 - \varepsilon. \tag{61}$$

By substituting Eq. (61) into the analytical solutions in *Case 1* and taking the limit as ε approaches zero, the analytical solutions can be reduced to the following equations: if $\overline{H}_{3c} > 0$,

$$\overline{H}_{1c} = +\overline{a}_s \cos\left(\overline{\xi}_s(\overline{t})\right), \tag{62a}$$

$$\overline{H}_{2c} = -\overline{a}_s \sin\left(\overline{\xi}_s(\overline{t})\right), \tag{62b}$$

$$\overline{H}_{3c} = +\sqrt{\frac{J_{3c}(J_{1c}-D)}{J_{1c}(J_{1c}-J_{3c})}} = \text{const.}, \tag{62c}$$

where $\overline{a}_s$ and $\overline{\xi}_s(\overline{t})$ can be expressed as:

$$\overline{a}_s = \pm\sqrt{\frac{D-J_{3c}}{J_{1c}-J_{3c}}}, \tag{63}$$

$$\overline{\xi}_s(\overline{t}) = \sqrt{\frac{(J_{1c}-D)(J_{1c}-J_{3c})}{J_{1c}J_{3c}}}(\overline{t}-\overline{t}_0). \tag{64}$$

If $\overline{H}_{3c} < 0$,

$$\overline{H}_{1c} = -\overline{a}_s \cos\left(\overline{\xi}_s(\overline{t})\right), \tag{65a}$$

$$\overline{H}_{2c} = -\overline{a}_s \sin\left(\overline{\xi}_s(\overline{t})\right), \tag{65b}$$

$$\overline{H}_{3c} = -\sqrt{\frac{J_{3c}(J_{1c}-D)}{J_{1c}(J_{1c}-J_{3c})}} = \text{const.}. \tag{65c}$$

Next, the case where the intermediate mass moment of inertia approaches the smallest moment of inertia is considered. The intermediate mass moment of inertia J_2 near the smallest mass moment of inertia J_3 can be expressed as follows using a small parameter ε, $|\varepsilon| \ll 1$:

$$J_2 = J_3 + \varepsilon. \tag{66}$$

By substituting Eq. (66) into the analytical solutions in *Case 2* and taking the limit as ε approaches zero, the analytical solutions can be reduced to the following equations: if $\overline{H}_{1c} > 0$,

$$\overline{H}_{1c} = +\sqrt{\frac{J_{1c}(D - J_{3c})}{J_{3c}(J_{1c} - J_{3c})}} = \text{const.}, \tag{67a}$$

$$\overline{H}_{2c} = -\overline{b}_s \sin\left(\overline{\eta}_s(\overline{t})\right), \tag{67b}$$

$$\overline{H}_{3c} = +\overline{b}_s \cos\left(\overline{\eta}_s(\overline{t})\right). \tag{67c}$$

where $\overline{b}_s$ and $\overline{\eta}_s(\overline{t})$ can be expressed as:

$$\overline{b}_s = \pm\sqrt{\frac{J_{1c} - D}{J_{1c} - J_{3c}}}, \tag{68}$$

$$\overline{\eta}_s(\overline{t}) = \sqrt{\frac{(J_{1c} - J_{3c})(D - J_{3c})}{J_{1c}J_{3c}}}\left(\overline{t} - \overline{t}_0\right). \tag{69}$$

If $\overline{H}_{1c} < 0$,

$$\overline{H}_{1c} = -\sqrt{\frac{J_{1c}(D - J_{3c})}{J_{3c}(J_{1c} - J_{3c})}} = \text{const.}, \tag{70a}$$

$$\overline{H}_{2c} = -\overline{b}_s \sin\left(\overline{\eta}_s(\overline{t})\right), \tag{70b}$$

$$\overline{H}_{3c} = -\overline{b}_s \cos\left(\overline{\eta}_s(\overline{t})\right). \tag{70c}$$

These solutions correspond with the axisymmetric solutions [3, 4].

Chapter 2, in part, is a reprint of the following published paper:

Rios, O., Ono, T., Murakami, H., and Impelluso, J. T., 2016, "An Analytical and Geometrical Study of the Dzhanibekov and Tennis Racket Phenomena," ASME Paper No. IMECE2016-65570. The thesis author was the principal researcher of this paper.

CHAPTER 3: NUMERICAL AND GEOMETRICAL RESULTS

3.1 Tennis Racket Experiment

The analytical solutions have now been obtained for the non-dimensional angular momentum components. Now, they are applied to the tennis racket phenomena and compared with the numerical solution by solving the non-dimensional Euler equations using the fourth-order Runge-Kutta method for discrete time with time increment Δt. For given values of $\overline{H}_{ic}(\overline{t})$, Eqs. (27a-c) give $\overline{H}_{ic}(\overline{t}+\Delta\overline{t})$, $i = 1,2,3$. Before doing so, the rigid body used in the analysis is presented.

As shown in Fig. 3.1, a moving coordinate frame is attached to the center of mass of the tennis racket. The mass and mass moment of inertia values used in the analysis are $m = 0.375\ kg$, $J_{1c} = 0.0185\ kg/m^2$, $J_{2c} = 0.0164\ kg/m^2$, $J_{3c} = 0.00121\ kg/m^2$.

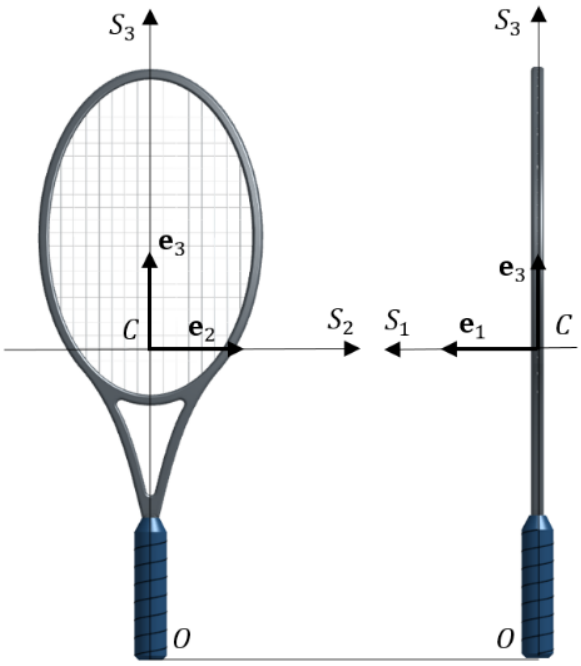

Figure 3.1: Tennis racket shown with the body attached coordinate frame and vector basis

To analyze the tennis racket phenomena, the racket will be spun with a large initial angular velocity around the $\mathbf{e}_2$-axis corresponding to the intermediate moment of inertia and small perturbations along the $\mathbf{e}_1$-and $\mathbf{e}_3$-axes

$$\omega_1(0) = \omega_3(0) = 0.001\, rad/s\,, \omega_2(0) = 5.0\, rad/s. \tag{71}$$

Before calculating the initial conditions for non-dimensional angular momentum from Eq. (22), the initial kinetic energy needs to be obtained using Eq. (16) and Eq. (71).

$$2K_0 = \left(J_1\left(\omega_1(0)\right)^2 + J_2\left(\omega_2(0)\right)^2 + J_3\left(\omega_3(0)\right)^2\right) = 0.41\,. \tag{72}$$

The initial conditions to be used in the numerical solution of Eqs. (27a-27c) are thus:

$$\begin{gathered} \overline{H}_{1c}(0) = 2.2561e-4, \\ \overline{H}_{2c}(0) = 1.0, \\ \overline{H}_{3c}(0) = 1.4756e-5. \end{gathered} \tag{73}$$

The numerical solution can now be obtained, but before presenting the solution, the analytical solution will be examined. As mentioned above, three distinct cases exist for the analytical solution, all dependent on the parameter D. To determine D, Eqs. (28) and (29) will be used:

$$D = J_{2c}\|\overline{H}_c(0)\|^2 = 1.64000000049927e-2 \tag{74}$$

From the value of D above, it can be seen that the analytical solution for *Case 2*, specifically the equations corresponding to $\overline{H}_{1c} > 0$, are needed to describe the tennis racket with the given initial conditions. Using the expression for $\overline{\eta}\left(\overline{t}\right)$ in Eqs. (51a-c), the analytical solution is obtained. Note, in the analytical solution, the issue of the time shift needs to be addressed. If the time shift is removed or set equal to zero ($\overline{t}_0 = 0$), the solution will not properly take into account the initial conditions for this particular problem. As can be noted

from Eq. (51b), without a time shift, $\overline{\eta}(\overline{t}) = 0$ at time $\overline{t} = 0$, thus making $\overline{H}_{2c} = 0$. Since the rotation is not solely about the smallest or largest moment of inertia, in which case $\overline{t}_0$ would be equal to zero, the angular momentum components need to be shifted so that the initial values match the initial conditions in Eq. (73). The time shift was found to be $\overline{t}_0 = 7.753\,\mathrm{s}$ from the initial condition and elliptic integral. The numerical and analytical solutions presented in Fig. 3.2 show great agreement between the analytical and numerical solution of each of the angular momentum components.

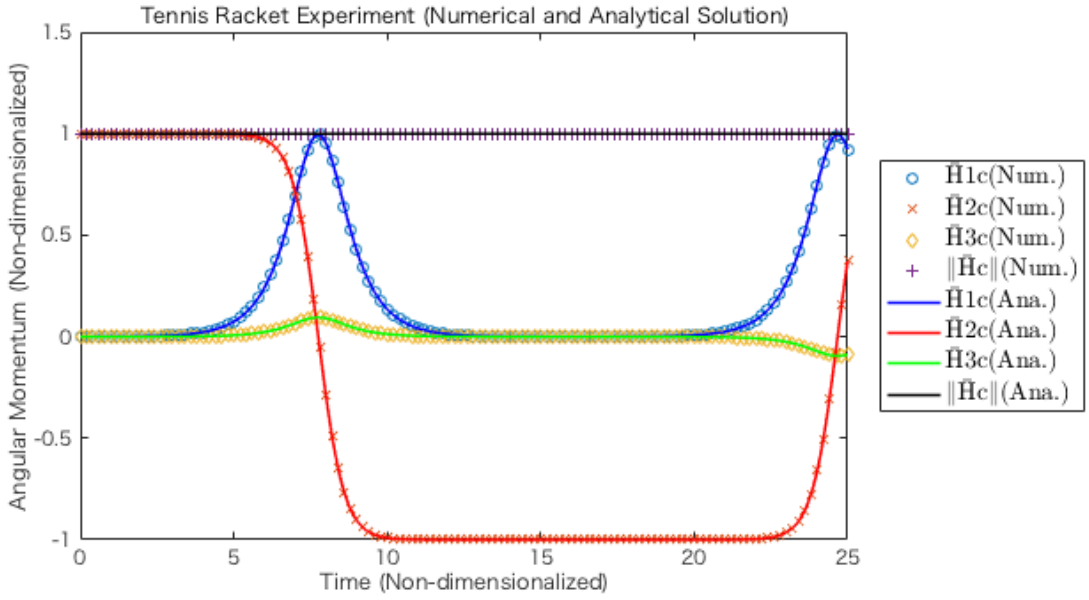

Figure 3.2: Plots of both the numerical and analytical solutions for the angular momentum components

3.2 Varying Moment of Inertia

Next, the effect of varying the mass moment of inertia is examined through the use of a satellite example. The progression of the trajectory and the period are analyzed as the rigid body changes geometry, varying the mass moment of inertia of the axis of rotation from the least to the intermediate value. As a specific example, a satellite released in space is presented as shown in Fig. 3.3 with an initial angular velocity around the $\mathbf{e}_2$-axis and small perturbations along the $\mathbf{e}_1$-and $\mathbf{e}_3$-axes. As the solar panels are deployed, the mass moment of inertia of the body changes. At the three positions shown in Fig. 3.3, the mass moment of inertia values are as follows:

$$J_1 = 0.9156e+4,\ J_2 = 0.3437e+4,\ J_3 = 0.8144e+4\ kg\ m^2, \tag{75a}$$

$$J_1 = 1.386e+4,\ J_2 = J_3 = 0.8619e+4\ kg\ m^2, \tag{75b}$$

$$J_1 = 1.782e+4,\ J_2 = 1.256e+4,\ J_3 = 0.8601e+4\ kg\ m^2. \tag{75c}$$

Although the rotational kinetic energy is conserved during the deployment, the angular velocities change.

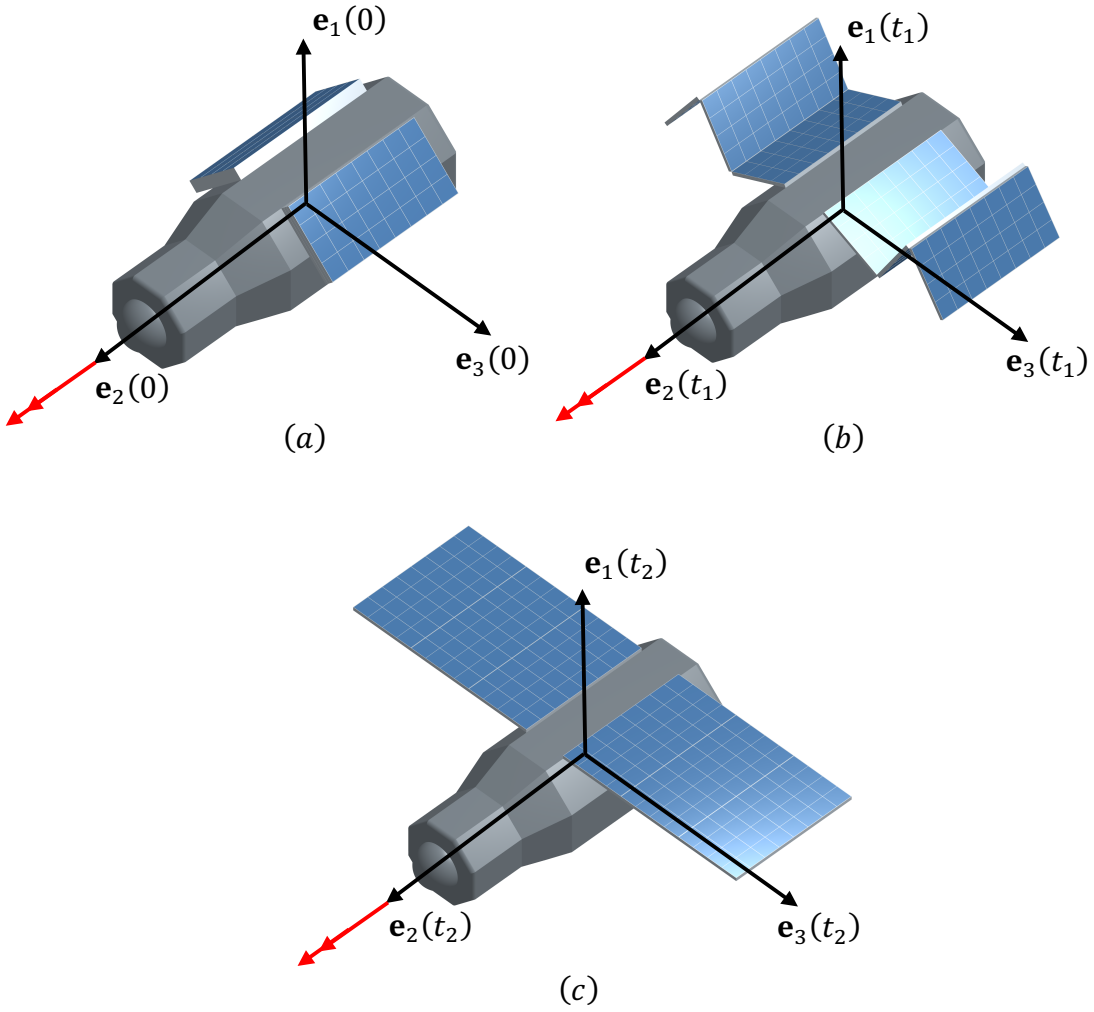

Figure 3.3: Satellite shown at three different configurations (a-c) with an initial angular velocity around the $\mathbf{e}_2$-axis deploying its solar panels, causing a change in the mass moment of inertia along the axis of rotation

The initial major angular velocity is given about the $\mathbf{e}_2$-axis of the satellite. For the satellite presented and from Eqs. (75a-c), the mass moment of inertia values obey, at $t = 0$, $J_1 > J_3 > J_2$ from Eqs. (75a-c). Since the rotation is currently about the smallest mass moment of inertia, a permanent state of rotation is expected. The trajectory of the satellite before the deployment of the solar panels can be obtained by the curve of intersection between

the angular momentum sphere and energy ellipsoid. Figure 3.4 shows the small curve of intersection along the $\overline{H}_{2c}$ axis in red.

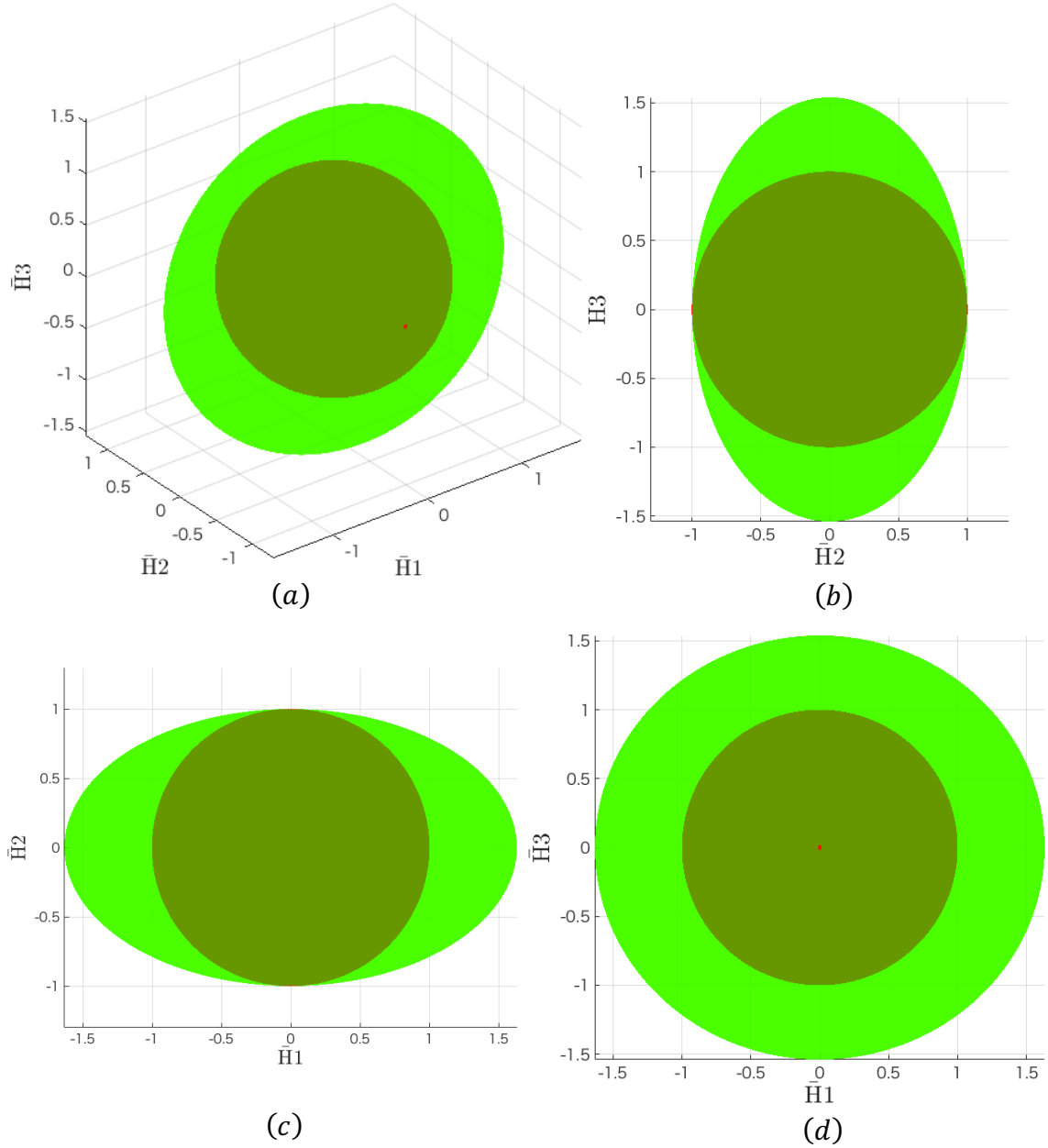

Figure 3.4: (a) Plotting of the energy ellipsoid (green) and the angular momentum sphere (red) and showing projections along the (b) $\overline{H}_3$-$\overline{H}_2$ (c) $\overline{H}_2$-$\overline{H}_1$ (d) $\overline{H}_3$-$\overline{H}_1$ plane for the initial satellite configuration shown in Fig. 3.3(a)

As the solar panels are deployed, the mass moment of inertia values change, as noted above in Eqs. (75a-c). The curve of intersection before the second configuration remains similar to the initial configuration, as the J_2-value is still the smallest moment of inertia. As the solar panels continue to unfold, the J_2-value goes from the smallest, to being equal to J_3 making an axisymmetric body, to the intermediate moment of inertia value. In Fig.3.5 below, the red line indicates the intersection between the energy ellipsoid and the angular momentum sphere when $J_2 = J_3$. When the value of J_2 becomes greater than that of J_3, a transition to a hyperbolic trajectory of the rigid body is seen, similar to that of the tennis racket. In Fig.3.6, the curve of intersection for the satellite with fully deployed solar panels is demonstrated.

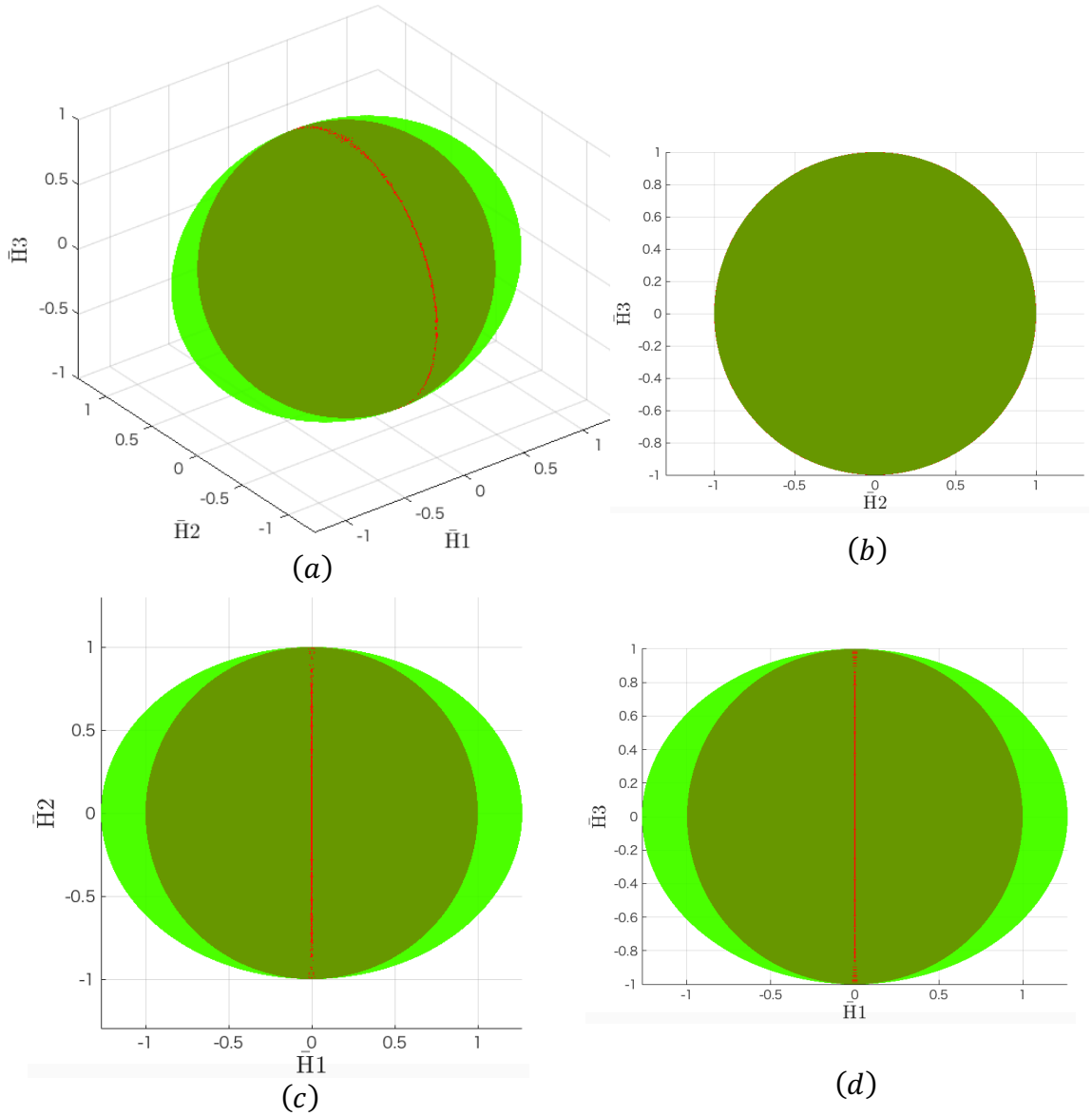

Figure 3.5: (a) Plotting of the energy ellipsoid (green) and the angular momentum sphere (red) and showing projections along the (b) $\overline{H}_3$-$\overline{H}_2$ (c) $\overline{H}_2$-$\overline{H}_1$ (d) $\overline{H}_3$-$\overline{H}_1$ plane for the second satellite configuration shown in Fig. 3.3(b)

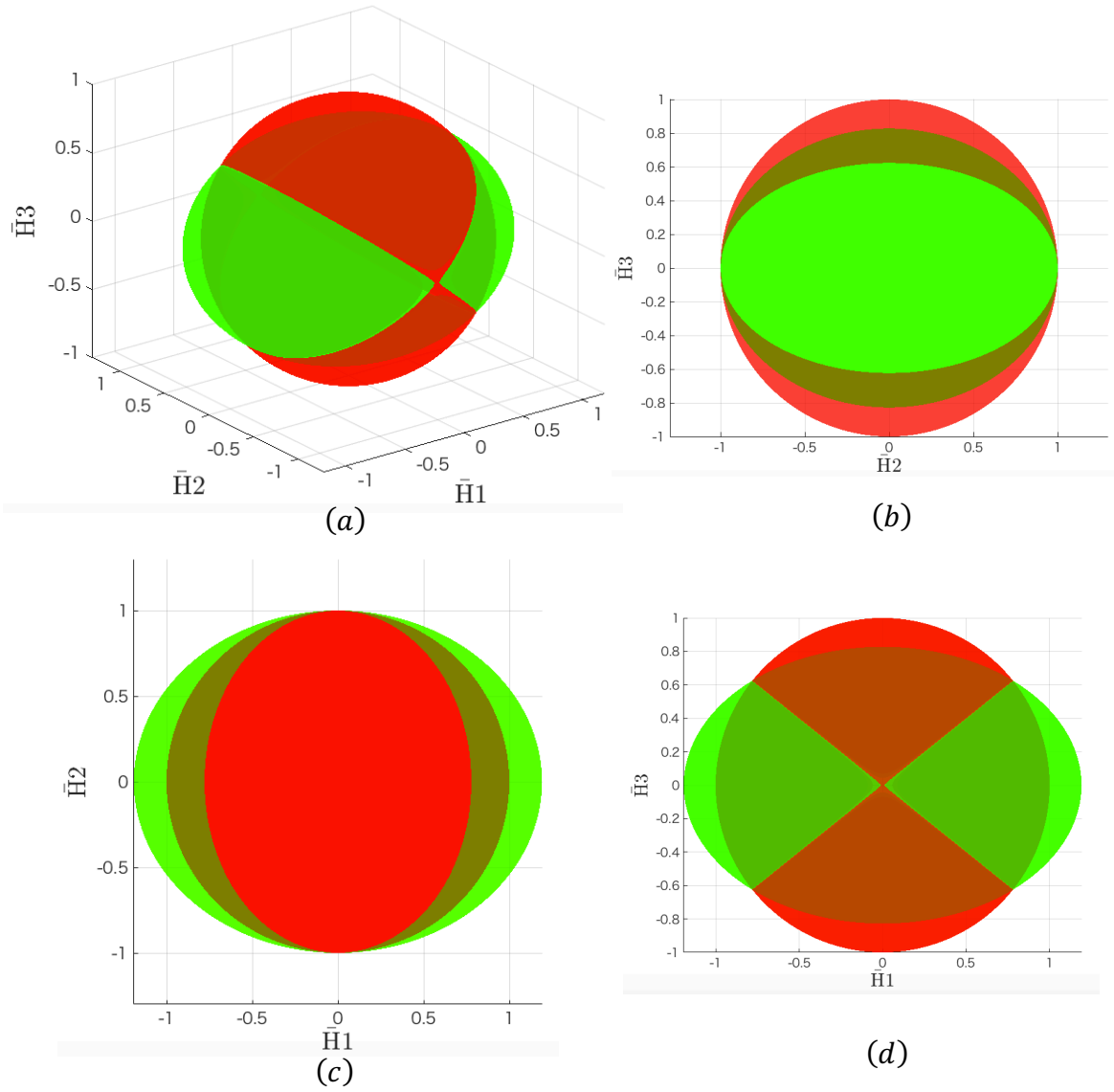

Figure 3.6: (a) Plotting of the energy ellipsoid (green) and the angular momentum sphere (red) and showing projections along the (b) $\overline{H}_3$-$\overline{H}_2$ (c) $\overline{H}_2$-$\overline{H}_1$ (d) $\overline{H}_3$-$\overline{H}_1$ plane for the final satellite configuration shown in Fig. 3.3(c)

To see the effect of J_2 on the trajectory after surpassing J_3 and becoming the intermediate value, the projections of the intersecting curve on the $\overline{H}_2 - \overline{H}_1$ plane, $\overline{H}_3 - \overline{H}_2$ plane, and $\overline{H}_3 - \overline{H}_1$ plane are plotted as the value of J_2 increases. The mass moment of inertia values when the satellite becomes an axisymmetric body are $J_2 = J_3 = 0.8619e + 4\ kg\ m^2$. As J_2 increases to the fully deployed value defined in Eq. (73c), the progression of the trajectory is shown in Fig. 3.7 below. The color of the intersecting curve changes from red to black as J_2 increases. From Fig. 3.4-3.6, the major semi-axis and the minor semi-axis of the energy ellipsoid along the body attached $\overline{H}_1$-axis and $\overline{H}_3$-axis change as varying the mass moment of inertia values. This observation can be confirmed from Eq. (28).

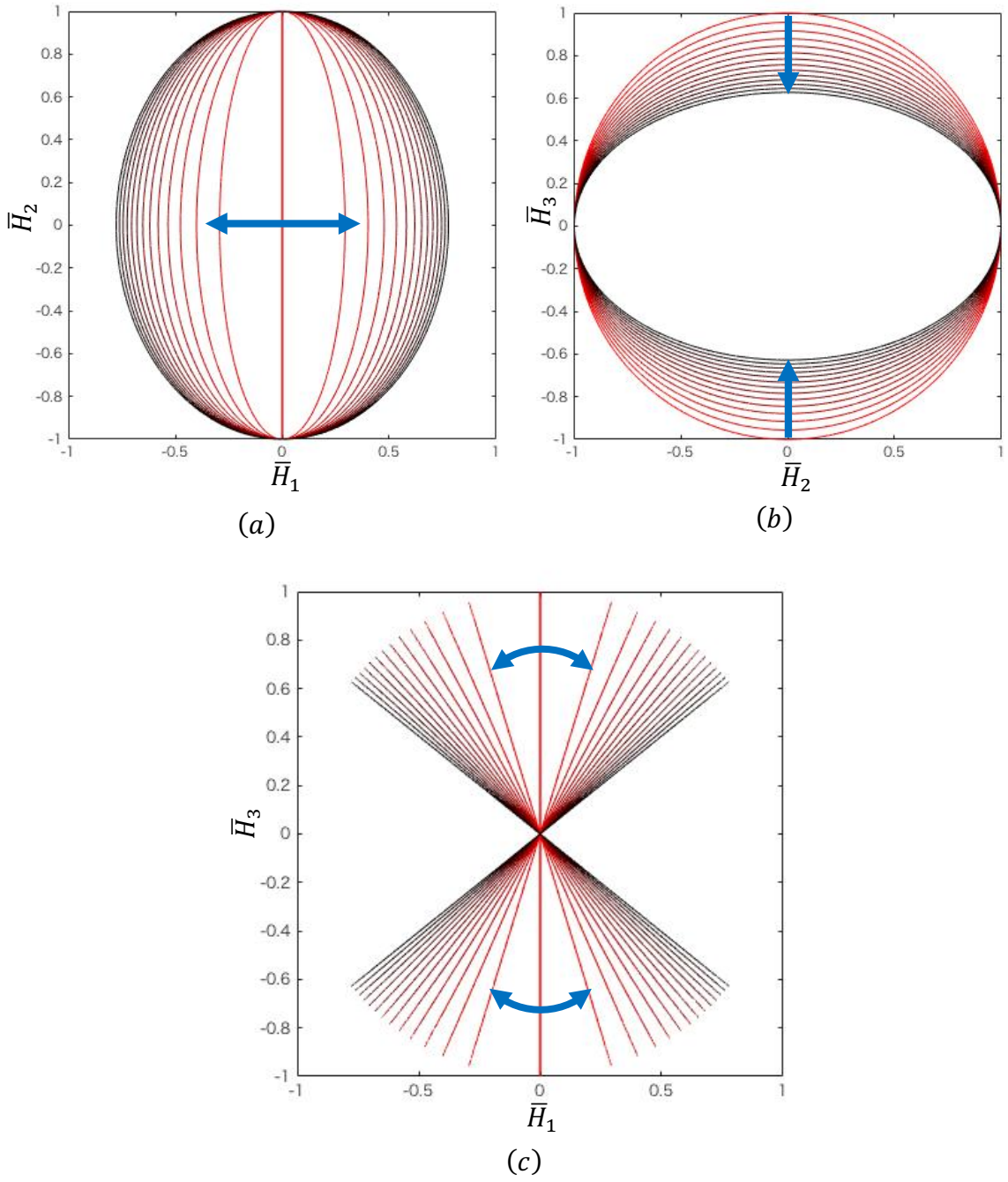

Figure 3.7: Projections along the (a) $\bar{H}_2$ - $\bar{H}_1$ (b) $\bar{H}_3$ - $\bar{H}_2$ (c) $\bar{H}_3$ - $\bar{H}_1$ plane of the progression of the trajectories as the deployment of the solar panels creates a variation of J_2 from $J_2 = J_3$ (red) to $J_1 > J_2 > J_3$ (black)

From Fig. 3.7, it is observed that as the satellite's solar panels are fully deployed and J_2 increases, the trajectory of the system becomes more sensitive initial disturbances. The progression of the non-dimensional period for the above trajectories is presented below in Fig. 3.8. The x-axis of the figure ranges from the point $J_2 = J_3$ to the final state shown in Fig. 3.3(c) above. As can be seen in the figure, as the solar panels deploy and near their final position, the body deviates from a permanent state of rotation to a trajectory with an exponentially decaying non-dimensional period.

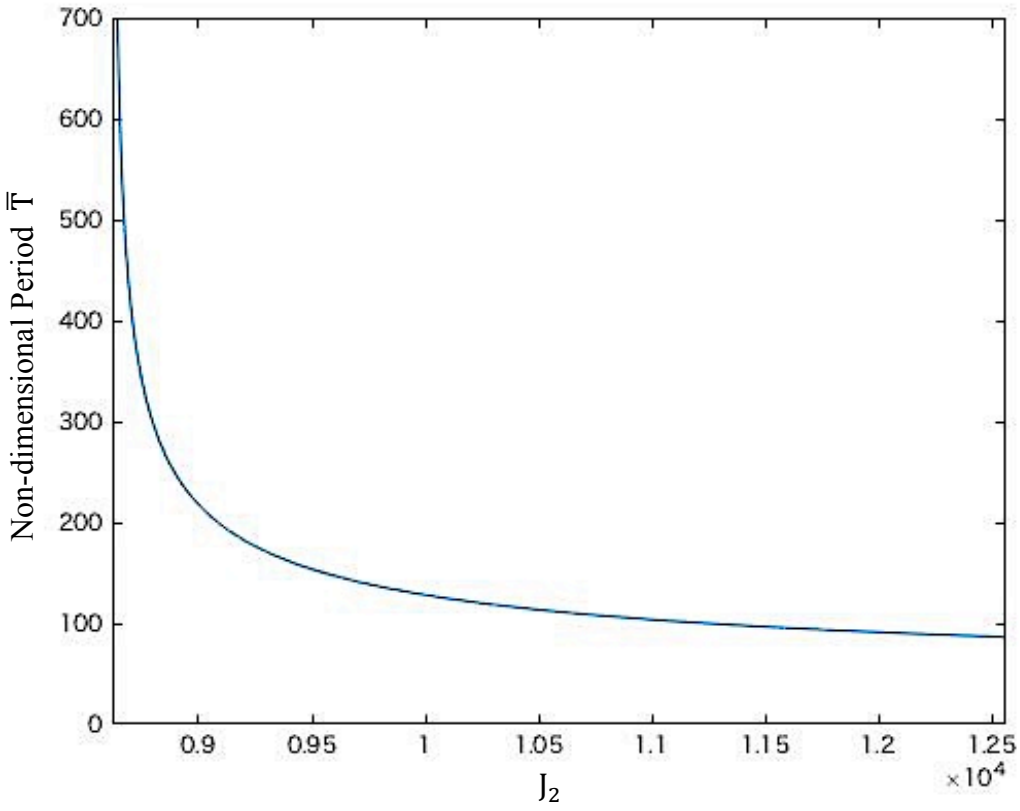

Figure 3.8: Plotting the progression of the non-dimensional period of the trajectory as the body goes from being axisymmetric to the final satellite configuration

In order to avoid or control an unstable rotation, global control is required rather than local control which can aggravate an already difficult situation.

As an opposing example to a rotating satellite, the rotation of an airplane can be considered. A flat spin, the rotation about the axis corresponding to the largest moment of inertia, is very dangerous and the hardest case to recover from if the rudder does not work sufficiently. The rotation about the axis corresponding to the smallest moment of inertia, which is related to spiral dive, also can lead to a serious situation due to significant increase in airspeed, rapid loss of altitude, and excessive loading because of improper recovery control application. However, in the rotation about the axis corresponding to the intermediate moment of inertia, the airplane will rotate in a periodic manner, making it is easier to control and recover. These are in contradiction to what is indicated in the case of the satellite and should be considered to control an unstable motion.

3.3 Numerical Integration of the Rotation Matrix

For an inertial frame observer, three-dimensional (3D) animations provide the necessary visual tool to connect and validate the numerical solutions. Since the components of the angular velocity and angular momentum vectors have been obtained with respect to the moving frame, Eq. (1) must be used to express the vector components with the inertial frame. To this end, in Eq. (1), the rotation matrix must be updated at each time for given values of angular velocity components.

From Eq. (4), reconstruction formula for $R(t)$ [6, 8] is expressed as:

$$\dot{R}(t) = R(t)\overleftrightarrow{\omega(t)}. \tag{76}$$

This equation can be integrated analytically from t to $t + \Delta t$ if the angular velocity remains constant $\omega(t) = \omega_0$. Using the constant angular velocity case, a numerical

integration scheme for time-dependent angular velocity cases can be developed. When the angular velocity is constant, the solution of Eq. (76) with initial value $R(0)$ becomes [7]

$$R(t) = R(0)\, exp(t\, \overleftrightarrow{\omega_0}) \tag{77}$$

where the matrix exponential is defined as

$$\begin{aligned} exp(t\, \overleftrightarrow{\omega_0}) &\equiv I_d + t\, \overleftrightarrow{\omega_0} + \frac{t^2}{2!}(\overleftrightarrow{\omega_0})^2 + \frac{t^3}{3!}(\overleftrightarrow{\omega_0})^3 + \cdots \\ &= \sum_{k=0}^{\infty} \frac{t^k}{k!}(\overleftrightarrow{\omega_0})^k \end{aligned} \tag{78}$$

In order for Eq. (77) to be useful, a simple expression for the matrix exponential is required. Eq. (78) is simplified using the Cayley-Hamilton theorem [11]. The simplified equation becomes

$$\begin{aligned} exp(t\, \overleftrightarrow{\omega_0}) \equiv I_d &+ \frac{\overleftrightarrow{\omega_0}}{\|\boldsymbol{\omega_0}\|} sin(t\, \|\boldsymbol{\omega_0}\|) \\ &+ \left(\frac{\overleftrightarrow{\omega_0}}{\|\boldsymbol{\omega_0}\|}\right)^2 \left(1 - cos(t\, \|\boldsymbol{\omega_0}\|)\right) \end{aligned} \tag{79}$$

and the derivation is presented in the Appendix.

While the constant angular velocity is not met under the Dzhanibekov phenomena, it can be applied by approximation to each time step of the Runge-Kutta integration. From this perspective, the midpoint integration method is adopted by using the mean value of the angular velocity, $\omega(t + \Delta t/2)$ as follows:

$$\omega(t + \Delta t/2) = \{\omega(t) + \omega(t + \Delta t)\}/2. \tag{80}$$

Assuming that the angular velocity is constant during the time step from t to $t + \Delta t$, Eq. (76) is integrated analytically for the initial value of $R(t)$ to find $R(t + \Delta t)$

$$R(t+\Delta t) = R(t)\, exp\{\Delta t\, \overleftrightarrow{\omega(t+\Delta t/2)}\}. \tag{81}$$

where Eq. (79) is used to evaluate the exponential matrix for $\omega_0 = \omega(t+\Delta t/2)$.

Chapter 3, in part, is a reprint of the following published paper:

Rios, O., Ono, T., Murakami, H., and Impelluso, J. T., 2016, "An Analytical and Geometrical Study of the Dzhanibekov and Tennis Racket Phenomena," ASME Paper No. IMECE2016-65570. The thesis author was the principal researcher of this paper.

CHAPTER 4: CONCLUSION

Euler's equations were expressed using the moving frame method, providing a clear distinction between a moving frame observer and an inertial frame observer. The Euler's equations were then non-dimensionalized and solved analytically together with expressions for the non-dimensional period of the trajectory. The numerical and analytical solutions for the tennis racket phenomena were compared and were shown to agree closely. Finally, the progression of the trajectory and the period were examined as the intermediate moment of inertia varied in a torque-free body. As a practical example, a satellite with an initial angular velocity deploying its solar panels was presented. As the solar panels are deployed, it was observed that a change in the trajectory and in the period of the satellite results in unwanted rotations.

APPENDIX

A.1 The Case with Constant Angular Velocity

For the computation of $(\overleftrightarrow{\omega_0})^k$ in Eq. (76), the characteristic equation of $\overleftrightarrow{\omega_0}$ is computed

$$\det(\overleftrightarrow{\omega_0} - \lambda I_d) = \det\begin{bmatrix} -\lambda & -\omega_{30} & \omega_{20} \\ \omega_{30} & -\lambda & -\omega_{10} \\ -\omega_{20} & \omega_{10} & -\lambda \end{bmatrix} \tag{A1}$$

$$= -\lambda^3 - \|\boldsymbol{\omega_0}\|^2\lambda = 0$$

where

$$\|\boldsymbol{\omega_0}\|^2 = (\omega_{10})^2 + (\omega_{20})^2 + (\omega_{30})^2 \tag{A2}$$

From Eq. (A1), the Cayley-Hamilton theorem gives

$$(\overleftrightarrow{\omega_0})^3 = -\|\boldsymbol{\omega_0}\|^2(\overleftrightarrow{\omega_0}) \tag{A3}$$

Using Eq. (A3), the right-hand side of Eq. (76) is expressed by I_d, $\overleftrightarrow{\omega_0}$, and $(\overleftrightarrow{\omega_0})^2$

$$exp(t\,\overleftrightarrow{\omega_0}) \equiv I_d + t\,\overleftrightarrow{\omega_0} + \frac{t^2}{2!}(\overleftrightarrow{\omega_0})^2 - \frac{t^3}{3!}\|\boldsymbol{\omega_0}\|^2(\overleftrightarrow{\omega_0})$$

$$-\frac{t^4}{4!}\|\boldsymbol{\omega_0}\|^2(\overleftrightarrow{\omega_0})^2 + \frac{t^5}{5!}\|\boldsymbol{\omega_0}\|^4(\overleftrightarrow{\omega_0}) \tag{A4}$$

$$+\frac{t^6}{6!}\|\boldsymbol{\omega_0}\|^4(\overleftrightarrow{\omega_0})^2 - \cdots$$

Furthermore, Eq. (A4) can be written as

$$
\begin{aligned}
exp(t\overleftrightarrow{\omega_0}) \equiv I_d & \\
& + \frac{\overleftrightarrow{\omega_0}}{\|\boldsymbol{\omega_0}\|}\left\{t\|\boldsymbol{\omega_0}\| - \frac{1}{3!}(t\|\boldsymbol{\omega_0}\|)^3 + \frac{1}{5!}(t\|\boldsymbol{\omega_0}\|)^5\right. \\
& \left. - \frac{1}{7!}(t\|\boldsymbol{\omega_0}\|)^7 + \cdots\right\} \\
& + \left(\frac{\overleftrightarrow{\omega_0}}{\|\boldsymbol{\omega_0}\|}\right)^2\left\{\frac{1}{2!}(t\|\boldsymbol{\omega_0}\|)^2 - \frac{1}{4!}(t\|\boldsymbol{\omega_0}\|)^4\right. \\
& \left. + \frac{1}{6!}(t\|\boldsymbol{\omega_0}\|)^6 - \frac{1}{8!}(t\|\boldsymbol{\omega_0}\|)^8 + \cdots\right\}
\end{aligned}
\tag{A5}
$$

Finally, Eq. (79) is found from the above equation.

REFERENCES

[1] Vladimirovich, F. Roman "About the Dzhanibekov Effect" YouTube video, February 11, 2013, https://www.youtube.com/watch?v=LzVItPwiQyI.

[2] Russell, Dan "Tennis Racket Theorem" YouTube video, March 5, 2010, https://www.youtube.com/watch?v=4dqCQqI-Gis.

[3] Wittenburg, J., 1977, Dynamics of Rigid Bodies, B. G. Teubner, Stuttgart, Germany.

[4] Wittenburg, J., 2008, *Dynamcs of Multibody Systems,* second edition, Springer, Berlin, Germany.

[5] Ashbaugh, M.S., Chicone, C.C. and Cushman, R.H., 1991. "The twisting tennis racket". *Journal of Dynamics and differential Equations*, *3*(1), pp.67-85.

[6] Murakami, H., Rios, Oscar., Impelluso T. J., 2016, "A Theoretical and Numerical Study of the Dzhanibekov and Tennis Racket Phenomena," *ASME Journal of Applied Mechanics*, Vol. 83, No. 11, paper 111006 (10 pages); also Murakami, H., Rios, Oscar., Impelluso T. J., 2015, "A Theoretical and Numerical Study of the Dzhanibekov and Tennis Racket Phenomena," *Proceedings of the ASME 2015 International Mechanical Engineering Congress & Exposition*, Paper IMECE2015-52374, ASME, New York.

[7] Frankel, T., 2012, The Geometry of Physics: An Introduction, 3rd ed., Cam- bridge University Press, New York.

[8] Murakami, H., 2013, "A Moving Frame Method for Multi-Body Dynamics," ASME Paper No. IMECE2013-62833.

[9] Poinsot, L., 1834, *Theorie Nouvelle de la Rotationn des Corps*, Paris.

[10] Abramowitz, M. and Stegun, I.A., 1964. "*Handbook of mathematical functions: with formulas, graphs, and mathematical tables"* (Vol. 55). Courier Corporation.

[11] Noble, B., and Daniel, J. W., 1977, Applied Linear Algebra, 2nd ed., Prentice- Hall, Englewood, NJ.